

## Deformation, Growth, and Order in Sheared Spinodal Decomposition

Daniel H. Rothman

*Department of Earth, Atmospheric, and Planetary Sciences, Massachusetts Institute of Technology,  
Cambridge, Massachusetts 02139*

(Received 25 September 1990)

The effect of hydrodynamics on growth is studied by numerical simulation of two-dimensional phase separation in a simple shear flow. The simulations are performed with a momentum-conserving lattice-gas model of an immiscible binary fluid. The results reveal that an anisotropic anomaly that was previously observed in experimentally obtained structure functions is due to a shear-induced, smecticlike ordering of the domains.

PACS numbers: 64.60.Cn, 05.70.Fh, 47.20.Hw, 47.55.Kf

In this Letter, I present evidence of ordered patterns in a numerical model of a system that is simultaneously held out of equilibrium by external forcing and subjected to a phase-separation transition by a deep quench. The work is inspired by recent experiments performed by Chan, Perrot, and Beysens<sup>1</sup> (CPB) in which a critical binary mixture is subjected to a weak shear flow and a thermal quench. The quench forces the system to undergo spinodal decomposition, the process by which an initially unstable mixture separates into its constituent components.<sup>2</sup> As these domains grow, they additionally become deformed due to the externally imposed shear. This phenomenon—namely, the interaction of hydrodynamics and growth—has recently captured considerable attention, resulting in theoretical predictions,<sup>3,4</sup> numerical simulations,<sup>5,6</sup> and other experimental observations.<sup>7</sup> Here I focus on a particular result of the CPB experiments: an unexpected anisotropy in the growing domains that was revealed by light scattering. The simulations reported in this Letter show this anisotropy to be the result of a smecticlike ordering due to hydrodynamic interactions between domains.

To simulate a phase-separating binary fluid subjected to a shear flow, I employ the *immiscible lattice gas* (ILG),<sup>8</sup> a variant of the single-species lattice gas<sup>9</sup> introduced for the simulation of the Navier-Stokes equations.

In the ILG, two species of particle, one “red” and the other “blue,” reside in two dimensions on a triangular lattice. Each particle has unit mass and can move with unit speed from site to site. When particles meet, they collide in a way that conserves mass, momentum, and color. Collisions are designed such that, for sufficiently large particle density  $d$  and minority concentration  $c$ , the mixed phase is unstable, phase separation occurs, and surface tension exists at interfaces. A phase diagram analogous to a classical spinodal curve may be constructed in the plane of  $d$  and  $c$ , where  $d$  is analogous to an inverse temperature.<sup>10</sup> Importantly, in addition to acting as a model of spinodal decomposition, the ILG also simulates hydrodynamics. In particular, the hydrodynamic theory<sup>11</sup> associated with the macroscopic behavior of single-species lattice-gas models applies equally to the macroscopic behavior of single-color regions of the ILG.<sup>8</sup> Detailed empirical studies additionally show that capillary phenomena observed in the ILG correspond to the behavior one expects from classical considerations, for both interfaces at rest<sup>8</sup> and moving interfaces.<sup>12,13</sup>

To further establish that the ILG is appropriate for a study of sheared growth, it is imperative to first validate its dynamical phase-separation behavior in the unsheared case. The basic quantity of interest is the *structure function*  $S(\mathbf{k}, t)$ , which is given for the ILG by the power spectrum

$$S(\mathbf{k}, t) = \frac{1}{n_x n_y} \left| \sum_x e^{-i2\pi\mathbf{k}\cdot\mathbf{x}} \{[\rho_b(\mathbf{x}, t) - \rho_r(\mathbf{x}, t)] - \rho(2c - 1)\} \right|^2. \quad (1)$$

Here  $\rho$  is the average number of particles per site,  $c$  is the average concentration of blue particles in the mixture,  $\rho_b(\mathbf{x}, t)$  and  $\rho_r(\mathbf{x}, t)$  are the number of blue particles and red particles, respectively, at time  $t$  at a site with coordinates given by  $\mathbf{x}$ ,  $\mathbf{k}$  is the discrete wave vector, and  $n_x$  and  $n_y$  are the number of lattice sites in the  $x$  direction and  $y$  direction, respectively.

Figure 1(a) displays an ensemble average of 1500 independent realizations of  $S(\mathbf{k}, t)$  at  $t=1000$  time steps after a deep quench. For these simulations,  $n_x = n_y = 128$ ,  $d = \rho/7 = 0.7$ , and  $c = 0.33$ . Each simulation was initiated with a two-dimensional homogeneous random

mixture with negligible net momentum. In the spectrum, there is a faint trace of the hexagonal symmetry of the triangular lattice<sup>14</sup> for large  $|\mathbf{k}|$  that should be insignificant at long-wavelength, hydrodynamic scales. We may thus conclude that the hydrodynamical aspects of ILG phase separation are isotropic.

Isotropy of  $S(\mathbf{k})$  allows circular averaging over  $k = |\mathbf{k}|$  to form  $\hat{S}(k)$ . Figure 1(b) displays  $\hat{S}(k, t)$ ,  $t=100, 200, \dots, 1000$ . If  $k_m$  is the value of  $k$  for which  $\hat{S}(k)$  is maximum, one expects that there is a scaling function  $F(k/k_m)$  such that<sup>2,15</sup>

$$\hat{S}(k, t) = A k_m^{-2}(t) F(k/k_m(t)), \quad (2)$$

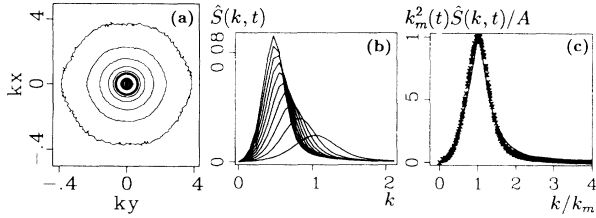


FIG. 1. (a) Contours of  $\log_{10} S(\mathbf{k})$  at  $t=1000$  time steps after quenching, in intervals of  $10^{1/2}$ .  $S(\mathbf{k})$  is an average computed from 1500 independent simulations. The highest contour level (near center) is bold. (b)  $\hat{S}(k, t)$  for  $t=100, \dots, 1000$ . The maximum of each curve grows with time. (c) Scaled structure functions  $A^{-1} k_m^2(t) \hat{S}(k, t)$  for  $t=100, \dots, 1000$ . Wave-number axes in (a) and (b) represent cycles per lattice unit.

where  $A$  is a time-independent constant chosen to make  $F(1)=1$ . Figure 1(c) displays the scaled structure functions  $A^{-1} k_m^2(t) \hat{S}(k, t)$  as a function of the time-dependent inverse length scale,  $k/k_m(t)$ ; one sees excellent adherence to the expected scaling. Moreover, the scaled structure functions are shown to qualitatively conform to a scaling function  $F$  recently proposed in Ref. 16.

To simulate sheared phase separation, plane Couette flow is constructed in a manner inspired by Ref. 17; see Fig. 2. On a lattice with  $L=n_y$  lattice units in the vertical direction and  $W=n_x\sqrt{3}/2=n_y\sqrt{3}$  lattice units in the horizontal direction, the average  $y$  velocity in the vertical column located at  $x=0$  is held at  $u_y=-u_0$ , while the average  $y$  velocity in the middle column, located at  $x=W/2$ , is held at  $u_y=u_0$ .<sup>18</sup> By making boundaries periodic in both directions, a V-shaped velocity profile,

$$u_y = \begin{cases} C(x - W/4), & 0 \leq x < W/2, \\ -C(x - 3W/4), & W/2 \leq x < W, \end{cases} \quad (3)$$

is obtained, where the shear rate  $C=4u_0/W$ .

Simulations of sheared growth are initialized with a homogeneous random mixture of density  $d$  and blue concentration  $c$ , with a velocity profile given by Eq. (3). To quantify the morphology of the resulting sheared domains, the structure functions  $S(\mathbf{k})$  are calculated by first computing the power spectrum  $S_L(\mathbf{k})$  of the left half of the simulation [i.e., by performing the summation in Eq. (1) only for  $0 \leq x < W/2$ ], then computing the analogous spectrum  $S_R(\mathbf{k})$  for the right half, and finally averaging<sup>19</sup> the two by setting  $S(\mathbf{k}) = \frac{1}{2} [S_L(\mathbf{k}) + S_R(-\mathbf{k})]$ .

Results are shown in Fig. 3, where for each case  $d=0.70$ ,  $c=0.35$ ,  $n_x=512$ ,  $n_y=256$ , and the viscosities are equal. The top row illustrates the time evolution of phase separation without shear ( $C=0$ ). In the middle row, the shear rate  $C=C_0=9.02 \times 10^{-4}$  results from setting  $u_0=0.10$ , whereas in the bottom row  $C=1.5C_0$ . Different initial conditions were chosen in each case. In both cases of shear,  $C$  is sufficiently small to correspond

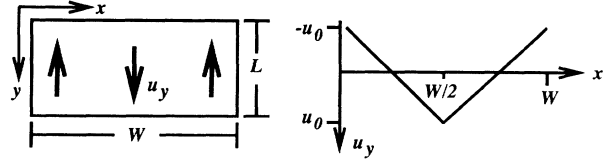


FIG. 2. Design of the numerical experiment (see text).

to the case called *weak shear*,<sup>1,3,4</sup> since the typical lifetime of a fluctuation is  $\sim 1$ .<sup>20</sup>

Figure 3 illustrates a striking dependence of these two-dimensional patterns on the shear rate  $C$ . For the case  $C=0$ , one sees, as expected, circular bubbles whose characteristic size grows with time while the number of bubbles decreases. The cases  $C > 0$ , on the other hand, show considerable deformation of the bubbles into elliptical domains, in which the major axes of the ellipses are oriented parallel to the direction that is approximately  $45^\circ$  from the vertical (flow) direction. This deformation and orientation is expected from elementary theoretical considerations:<sup>21</sup> The bubbles are simply stretched along the principal (extensional) axis of strain. A surprising result, however, is the *positional* ordering of the bubbles that is evident in addition to this orientational ordering. Particularly at late times, the bubbles fall into ordered stacks. The stacks themselves are separated at a distance  $\lambda(t)$  comparable to the length of the major axis of the average elliptical bubble. Indeed, at late times a “bubble wave” roughly proportional to  $\cos[2\pi\mathbf{k}_0(t) \cdot \mathbf{x}]$

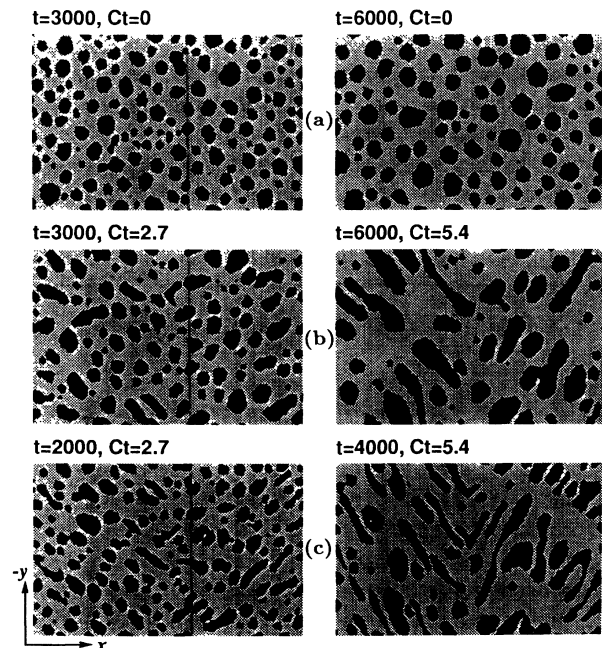


FIG. 3. Patterns of the domains at two different times after quenching. (a) No shear,  $C=0$ . (b)  $C=C_0=9.02 \times 10^{-4}$ . (c)  $C=1.5C_0$ . Time  $t$  is in time steps;  $Ct$  is shear strain.

$+\phi]$  may be perceived, where the wave vector  $\mathbf{k}_0(t) \approx \lambda^{-1}(t)(\pm \hat{\mathbf{x}} - \hat{\mathbf{y}})/\sqrt{2}$  and  $\phi$  is an arbitrary phase. Here the minus sign of the unit vector  $\hat{\mathbf{x}}$  refers to the left half of the simulation, and the plus sign to the right.

Further, and more convincing, evidence of these ordered structures is obtained from the structure functions. Figure 4 contains contour plots of  $S(\mathbf{k}, t)$  corresponding to each late-time depiction of real space in Fig. 3; here, however, each plot of  $S(\mathbf{k}, t)$  was computed by averaging over an ensemble of forty independent simulations. Two features stand out when comparing  $S(\mathbf{k}, t)$  for  $C > 0$  to the corresponding  $S(\mathbf{k}, t)$  for  $C = 0$ . First, the spectra are now elliptical in shape, rather than circular. Second, there is a severe drop in spectral power in a direction roughly aligned with the major axes of these elliptical spectra. The former feature is expected: These ellipses are simply the reciprocal-space depiction of the elliptical bubbles in real space. The second feature is a quantitative measure of the ordering of the bubbles in real space. If the elliptical bubbles were randomly positioned, contours of the spectral power in reciprocal space would be unbroken ellipses. However, the appearance of the bubble wave approximated by  $\cos[\mathbf{k}_0(t) \cdot \mathbf{x} + \phi]$  creates anomalously large spectral power in the vicinity of  $\mathbf{k} = \pm \mathbf{k}_0(t)$  in reciprocal space. Because the total spectral power  $\sum_{\mathbf{k}} S(\mathbf{k}, t)$  is approximately<sup>22</sup> a constant of time, the creation of this large spectral component near  $\mathbf{k} = \pm \mathbf{k}_0(t)$  leads to a concomitant depletion of power in the direction approximately orthogonal to it.

This dropoff of power near the major axes of the elliptical power spectra was also observed in the analogous light-scattering patterns obtained in reciprocal space in the CPB experiments. Thus the CPB experimental observations lend additional credence to the ordered structures obtained in real space in the ILG simulations.

A simple argument offers insight into the physical processes responsible for the generation of these ordered patterns. Consider two identical elliptical bubbles in a shear flow  $u_y = Cx$ , both with major axes of length  $\lambda$  oriented at an angle  $\theta$  to the flow direction. The bubbles are placed in the flow such that the line  $x = 0$  is halfway

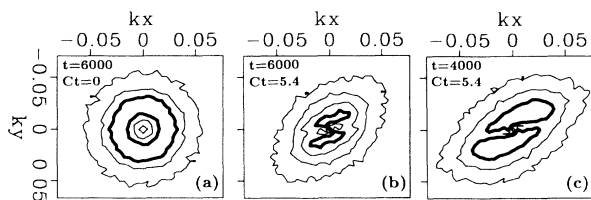


FIG. 4. Contours of  $\log_{10} S(\mathbf{k})$  computed by averaging spectra from 40 independent simulations. The contour interval is  $10^{1/2}$ ; the lowest contour in each plot is the same and the highest contour in each plot is bold. Times  $t$  and shear rates  $C$  in (a)–(c) correspond to those of the real-space patterns depicted at the later time in (a)–(c), respectively, of Fig. 3. All  $k_x, k_y$  axes are scaled identically.

between their centers of mass. Thus one bubble flows at velocity  $u_y = v_0$  while the other bubble flows at velocity  $u_y = -v_0$ . If the bubbles are separated in the  $x$  direction such that  $2C^{-1}v_0 > \lambda \sin\theta$ , they simply flow past each other at velocity  $u_y = 2v_0$ . However, if the bubbles are sufficiently closely spaced such that  $2C^{-1}v_0 \ll \lambda \sin\theta$ , they interact significantly as they approach each other. Specifically, if the bubbles are approximated by two flat surfaces of length  $\lambda$  separated by a distance  $h \ll \lambda$  and moving towards each other at speed  $\dot{h}$ , then for  $\rho h \dot{h} / \mu \ll 1$ , lubrication theory<sup>23</sup> shows that the rate of approach slows down such that  $\dot{h} \propto h^3 / \mu \lambda^3$ , where  $\mu$  is the shear viscosity. Stacks of bubbles thus form by a succession of similar near collisions that are relatively frozen in time. These stacks last until either (1) bubbles coalesce, and begin to form a new stack at a larger scale, or (2) the bubbles slide past one another due to the shear.

The uneven distribution of power in the elliptical  $S(\mathbf{k})$  is thus a measure of the additional time during which bubbles are “locked” in place as the shear flow causes them to flow in each other’s path. Because a lower surface tension  $\sigma$  allows bubbles to become flatter upon mutual approach, and a greater viscosity enhances the slowdown in  $\dot{h}$ , the ordering effect should increase as the capillary number  $Ca = C\lambda\mu \sin\theta / \sigma$  increases. A comparison of the two nonzero shear rates in Fig. 3 indicates the effect of increasing  $Ca$ : Ordering is initiated at earlier times due to greater deformation of the bubbles. In Fig. 3(b),  $Ca \approx 0.2$  at the later time, while in Fig. 3(c),  $Ca \approx 0.3$ .

Formally, the pattern of the sheared domains observed here is analogous to the structure of certain smectic liquid crystals.<sup>24</sup> The patterns are ordered in the direction given by the wave vector  $\mathbf{k}_0$ , but relatively disordered in the orthogonal direction. Qualitatively similar ordered structures have been observed in simulations of sheared colloidal suspensions<sup>25</sup> but the time-dependent behavior here is considerably different due to the concurrent phase separation. Unusual rheological properties, already indicated in Refs. 5 and 26, are expected due to competition between capillary and viscous forces. A preliminary study shows that the effective viscosity of the phase-separating mixture displays a complex time dependence in which the maximum excess viscosity is coincident with the maximal ordering of the domains.<sup>27</sup>

I thank D. Beysens, F. Perrot, Y. Pomeau, S. Zaleski, and G. Zanetti for instructive discussions. This work was supported by NSF Grant No. EAR-8817027 and by the sponsors of the MIT Porous Flow Project.

<sup>1</sup>C. K. Chan, F. Perrot, and D. Beysens, *Phys. Rev. Lett.* **61**, 412 (1988); F. Perrot, C. K. Chan, and D. Beysens, *Europhys. Lett.* **9**, 65 (1989); C. K. Chan, F. Perrot, and D. Beysens, *Phys. Rev. A* (to be published).

<sup>2</sup>J. D. Gunton, M. San Miguel, and P. S. Sahni, in *Phase*

*Transitions and Critical Phenomena*, edited by C. Domb and J. L. Lebowitz (Academic, New York, 1983).

<sup>3</sup>T. Imaeda, A. Onuki, and K. Kawasaki, *Prog. Theor. Phys.* **71**, 16 (1984).

<sup>4</sup>A. Onuki, *Phys. Rev. A* **34**, 3528 (1986); *Int. J. Thermophys.* **10**, 293 (1989).

<sup>5</sup>T. Ohta, H. Nozaki, and M. Doi, *Phys. Lett. A* **145**, 304 (1990).

<sup>6</sup>C. K. Chan and L. Lin, *Europhys. Lett.* **11**, 13 (1990).

<sup>7</sup>T. Hashimoto, T. Takebe, and S. Suehiro, *J. Chem. Phys.* **88**, 5874 (1988).

<sup>8</sup>D. H. Rothman and J. M. Keller, *J. Stat. Phys.* **52**, 1119 (1988).

<sup>9</sup>U. Frisch, B. Hasslacher, and Y. Pomeau, *Phys. Rev. Lett.* **56**, 1505 (1986).

<sup>10</sup>D. H. Rothman and S. Zaleski, *J. Phys. (Paris)* **50**, 2161 (1989).

<sup>11</sup>U. Frisch, D. d'Humières, B. Hasslacher, P. Lallemand, Y. Pomeau, and J.-P. Rivet, *Complex Systems* **1**, 648 (1987); *S. Wolfram, J. Stat. Phys.* **45**, 471 (1986); L. Kadanoff, G. McNamara, and G. Zanetti, *Phys. Rev. A* **40**, 4527 (1989); G. Zanetti, *Phys. Rev. A* **40**, 1539 (1989).

<sup>12</sup>D. H. Rothman, *J. Geophys. Res.* **95**, 8663 (1990).

<sup>13</sup>A. K. Gunstensen and D. H. Rothman, *Physica D* (to be published).

<sup>14</sup>Plot axes in all figures are rescaled by factors of  $\sqrt{3}/2$  when necessary to prevent vertical exaggeration.

<sup>15</sup>J. Marro, J. L. Lebowitz, and M. H. Kalos, *Phys. Rev. Lett.* **43**, 282 (1979); J. L. Lebowitz, J. Marro, and M. H. Kalos, *Acta Metall.* **30**, 297 (1982); H. Furukawa, *Adv. Phys.* **34**, 703

(1985).

<sup>16</sup>P. Fratzl and J. L. Lebowitz, *Acta Metall.* **37**, 3245 (1989).

<sup>17</sup>L. Kadanoff, G. McNamara, and G. Zanetti, *Complex Systems* **1**, 790 (1987).

<sup>18</sup>The velocities at  $x=0$  and  $x=W/2$  are held constant in a time-averaged sense, by randomly adding momentum (but neither mass nor color) when necessary.

<sup>19</sup>Note that the averaging of the spectra  $S_L$  and  $S_R$  preserves the orientation of the bubbles on the left half of the simulation but reverses them ( $x \leftarrow -x$ ) on the right. In the remainder of the discussion the orientation of the left half is always assumed.

<sup>20</sup>Based on a bubble size that traverses a lateral length  $l=W/8$ , the largest Reynolds number in the simulations is  $Re = |g(\rho)|\rho Cl^2/\mu \approx 15$ , where here the dynamic viscosity  $\mu = 1.43$  and  $|g(\rho)| = 0.81$  (Ref. 13). Nonunitary  $g$  formally breaks Galilean invariance (Ref. 9) but the small  $Re$  of these simulations (and results from empirical tests at  $d=0.50$ , where  $g=Re=0$ ) indicates that this is inconsequential.

<sup>21</sup>G. I. Taylor, *Proc. Roy. Soc. London A* **146**, 501 (1934); J. M. Rallison, *Annu. Rev. Fluid Mech.* **16**, 45 (1984).

<sup>22</sup>The sum, usually taken to be constant (Ref. 15), varies by a few percent in the ILG because of mixing at interfaces.

<sup>23</sup>O. Reynolds, *Philos. Trans. Roy. Soc.* **177**, 157 (1886).

<sup>24</sup>P.-G. de Gennes, *The Physics of Liquid Crystals* (Clarendon, Oxford, 1974).

<sup>25</sup>J. F. Brady and G. Bossis, *Annu. Rev. Fluid Mech.* **20**, 111 (1988); M. Doi and D. Chen, *J. Chem. Phys.* **90**, 5271 (1989).

<sup>26</sup>A. Onuki, *Phys. Rev. A* **35**, 5149 (1987).

<sup>27</sup>D. H. Rothman, *Europhys. Lett.* (to be published).

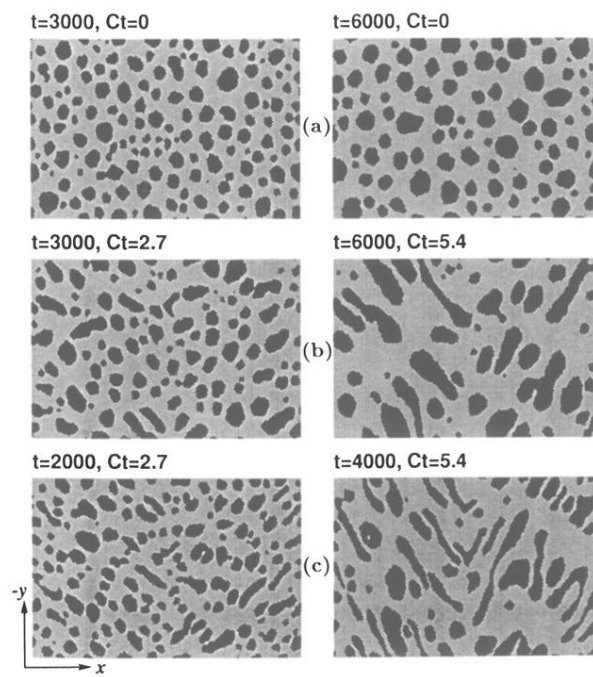


FIG. 3. Patterns of the domains at two different times after quenching. (a) No shear,  $C=0$ . (b)  $C=C_0=9.02 \times 10^{-4}$ . (c)  $C=1.5C_0$ . Time  $t$  is in time steps;  $Ct$  is shear strain.